Theoretical study of Piezotronic Metal-Insulator-Semiconductor Tunnel Devices

To cite this article before publication: Qiyuan Zhang *et al* 2018 *J. Phys. D: Appl. Phys.* in press https://doi.org/10.1088/1361-6463/aad067

Theoretical study of Piezotronic Metal-Insulator-Semiconductor Tunnel Devices

Qiyuan Zhang [1, †], Xiaolong Feng [1, †], and Lijie Li [2,*]

[1] *School of Physics, Experimental High School, University of Electronic Science and Technology of China, Chengdu 610054*

[2] *Multidisciplinary Nanotechnology Centre, College of Engineering, Swansea University, Swansea, SA1 8EN, UK*

[†] These authors contributed equally to this work.

[*] To whom correspondence should be addressed, E-mail: L.Li@swansea.ac.uk

Abstract

Piezotronics has been an emerging concept coupling piezoelectric and semiconducting properties with potential applications in sensors, flexible electronics and nanoelectromechanical systems (NEMS). Piezoelectric field is created under an applied strain, which controls the carrier generation, transport, separation or recombination processes at the interface or junction of the semiconductor devices. Based on the piezotronic theory, we present a one-dimensional model for the metal-insulator-semiconductor (MIS) tunnel diode based on the piezoelectric semiconductor. Analytical solutions of piezoelectric modulated tunneling are described to reveal the piezotronic effect on the MIS tunnel junction. Numerical simulation of the carrier transport properties is provided for demonstrating the piezotronic effect on MIS tunnel devices.

Keyword: piezotronics, piezoelectric semiconductor, metal-insulator-semiconductor structure, tunneling current

1. Introduction

Since the first nanogenerator was created using the piezoelectric zinc oxide nanowires, [1] piezoelectric semiconductor have attracted much attention for energy harvesting and pieozotronic devices. Due to the coupling of piezoelectric and semiconductor properties, previous experiments showed that bending the piezoelectric material can change the electric conductance [2] and modify the metal-semiconductor contact from Ohmic to Schottky contact [3]. All these high-performance devices contributed to a new field named as piezotronics [4-6], which aims at the coupling of piezoelectric and semiconducting properties, and applying the piezoelectric field induced by the strain to control the charge transport at the interface or junction. The piezotronic effect has been employed to achieve various devices, such as high-sensitivity strain sensors [7, 8], high output-power nanogenerator [9, 10] and piezotronic transistors [11, 12]. Large-array three-dimensional circuits based on piezotronic transistors has been reported in [11], and a nanowire light-emitting diode-based sensor array has been presented in [13]. Recently, piezoelectricity of the two-dimensional materials MoS_2 has been demonstrated in [14].

Piezoelectric field under an applied strain can control carrier transport. Based on metal semiconductor structure, gauge factor of the piezotronic strain sensor can reach up to 1250. [3] The gauge factor is higher than Si nanowires ~320 [15] and carbon nanotubes strain sensors~1000. [16] For strain controlled piezoelectric semiconductor devices, previous reports have provided models for p-n junctions, metal-semiconductor and heterojunctions based on semiconductor physics.

Typical building blocks of semiconductor devices include p-n junction, metal-semiconductor (MS) contact, MIS structure, and heterojunction. MIS structure has become very attractive due to its superior electronic properties, which leads to many promising applications, such as MIS solar cells [17, 18], photodetectors [19, 20], sensors [21] and memories [22, 23]. Taking the MIS solar cells as an example, the dark current can be reduced by increasing the effective metal-semiconductor barrier height or reducing the majority carrier concentration at the semiconductor surface [24, 25]. Metal-oxide-semiconductor (MOS) is one of MIS structures which uses the oxide layer as the gate insulator. It also has the advantage of easy integration with conventional semiconductors compared with p-n junctions.

In this paper, one dimensional metal-insulator-piezoelectric semiconductor contacts with an

ultrathin insulating layer are investigated under mechanical strains. Different from the conventional external transverse field modulation, this approach utilizes the inner parallel piezoelectric field to tune the transport properties at the interface.

2. Device model of piezotronic junction based on metal-insulator-semiconductor

According to previous theoretical studies [26], Poisson's equation, current transports equation, continuity equation, and the piezoelectric equation are set up to describe the piezotronic devices [27-31]. The MIS structure has important applications, the physics of the MIS structure has been intensively studied [32-42]. Here in this section we propose a simplified model to demonstrate the piezotronic effect for the MIS structure.

From the band diagram shown in Figure 1, the potential difference for the insulator can be given by

$$\Delta = \frac{E_g}{q} + \chi_s - \phi_m - \phi_p - \psi_s + V \quad (1)$$

where E_g is the semiconductor bandgap, χ_s denotes the affinity of the semiconductor, ϕ_m represents the metal work function, ϕ_p is the potential difference between the majority-carrier Fermi level and the valence band, ψ_s is the potential across the semiconductor and V denotes the applied voltage.

For simplicity, surface states, work function differences and other anomalies are neglected. The semiconductor is grounded, and a positive voltage is applied to the metal. It is assumed that the semiconductor is working in thermal equilibrium and direct tunneling is the dominant tunneling mechanism at the interface. Therefore, the difference between the electron and hole quasi-Fermi levels is neglected. Thus,

$$\Delta = -\psi_s + V \quad (2)$$

According to the Gauss's law, we have

$$\Delta = E_i d_i = d_i \frac{Q_M}{\varepsilon_i} \quad (3)$$

where E_i is the electric field inside the insulator, Q_M is the charge on the metal, d_i is the insulator thickness and ε_i is the permittivity of the insulator. For charge neutrality, it is required that

$$Q_M + Q_S + Q_{piezo} = 0 \quad (4)$$

where Q_S is the charge on the semiconductor surface due to the ionized acceptor and Q_{piezo} is the piezoelectric charge. Thus, equations can be given by

$$\Delta = -d_i \frac{(Q_S + Q_{piezo})}{\varepsilon_i} \quad (5\text{-a})$$

$$Q_S = -qN_A W_{Dp} \quad (5\text{-b})$$

$$Q_{piezo} = q\rho_{piezo} W_{piezo} \quad (5\text{-c})$$

Assuming the depletion approximation and completed ionization inside the depletion region, we proceed to calculate the field and potential distribution. The potential $\psi_s(x)$ inside the semiconductor as a function of distance can be obtained by solving the one-dimensional Poisson's equation

$$\frac{d^2\psi_s(x)}{dx^2} = -\frac{dE}{dx} = -\frac{\rho(x)}{\varepsilon} = -\frac{q[p(x) - n(x) - N_A(x) + \rho_{piezo}(x)]}{\varepsilon} \quad (6)$$

where $\rho(x)$ is the charge density as shown in Figure 1a, $N_A(x)$ is the density of the acceptor, $\rho_{piezo}(x)$ is the density of the piezoelectric charges. By integrating the Poisson equation, we can obtain the electric field distribution inside the semiconductor.

$$E(x) = -\frac{qN_A(x - W_{Dp})}{\varepsilon_s} + \frac{q\rho_{piezo}(x - W_{piezo})}{\varepsilon_s} \quad (0 \le x \le W_{piezo}) \quad (7\text{-a})$$

$$E(x) = -\frac{qN_A(x - W_{Dp})}{\varepsilon_s} \quad (W_{piezo} \le x \le W_{Dp}) \quad (7\text{-b})$$

By setting $\psi_s(N_A) = 0$, we can get the potential distribution across the contact as shown in Figure 1(c).

$$\psi(x) = \frac{qN_A(x - W_{Dp})^2}{2\varepsilon_s} - \frac{q\rho_{piezo}(x - W_{piezo})^2}{2\varepsilon_s} \quad (0 \le x \le W_{piezo}) \quad (8\text{-a})$$

$$\psi(x) = \frac{qN_A(x - W_{Dp})^2}{2\varepsilon_s} \quad (W_{piezo} \le x \le W_{Dp}) \quad (8\text{-b})$$

Thus, the band bending of the semiconductor valence band can be given by

$$\psi_s = \psi(0) = \frac{q}{2\varepsilon_s}(N_A W_{Dp}^2 - \rho_{piezo} W_{piezo}^2) \quad (9)$$

where ε_s is the permittivity of the semiconductor, N_A is the acceptor concentration, ρ_{piezo} is the density of the piezoelectric charges, W_{piezo} is the width of the piezoelectric charges distribution region and W_{DP} is the depletion layer width in the semiconductor.

According to the depletion assumptions of the analytical model, the majority carriers have been removed in the depletion region. Thus, the piezo-charges are not screened by carriers in depletion region in this case. For the piezotronic MIS structure, piezoelectric charges change the energy band and building-in potential in the MIS structure. The carries redistribution is neglected in our simplified analytical model.

3. Current-voltage characteristics of simplified piezotronic metal-insulator-semiconductor tunnel junction

According to typical tunneling current model [43], and previous works by Gray [44], Card and Rhoderick [33, 34], Doghish [40], the hole and electron tunneling currents can be written as

$$J_{nt} = A_n^* T^2 \exp\left(-\chi_n^{\frac{1}{2}} d_i\right)\left[\exp\left(-\frac{E_{c0}-E_{fm}}{kT}\right) - \exp\left(-\frac{E_{c0}-E_{fs}}{kT}\right)\right] =$$

$$A_n^* T^2 \exp\left(-\chi_n^{\frac{1}{2}} d_i\right)\exp\left(-\frac{E_g}{kT}\right)\exp\left(\frac{q\phi_p+q\psi_s}{kT}\right)\left[\exp\left(\frac{qV}{kT}\right)-1\right] \quad (10\text{-a})$$

$$J_{pt} = A_p^* T^2 \exp\left(-\chi_p^{\frac{1}{2}} d_i\right)\left[\exp\left(-\frac{E_{fs}-E_{v0}}{kT}\right) - \exp\left(-\frac{E_{fm}-E_{v0}}{kT}\right)\right] =$$

$$A_p^* T^2 \exp\left(-\chi_p^{\frac{1}{2}} d_i\right)\exp\left(-\frac{q\phi_p+q\psi_s}{kT}\right)\left[1-\exp\left(-\frac{qV}{kT}\right)\right] \quad (10\text{-b})$$

where A_n^* and A_p^* are effective Richardson constants for electrons and holes, χ_n and χ_p are effective barrier heights for electrons and holes tunneling into metal. The total current density can be given by

$$J_t = J_{pt} + J_{nt} \quad (11)$$

It indicates that the piezoelectric charges can tune the tunneling current J_t by changing the surface potential ψ_s of semiconductor.

Figure 2a shows the current-voltage characteristics of an ideal metal-insulator- GaN contact at different strains ranging from -0.08% to 0.08%. The calculated tunneling current density varies as the strain changes, demonstrating the modulation of the piezoelectric charges. It is seen that a tensile strain leads to a reduced current density, which matches with the theory described in previous sections. The current density remains almost unchanged for voltages of less than 0.35V and demonstrates a significant difference at 0.45V for various strain values. It is also worth mentioning that the relation between the strain and the current density at a certain voltage e.g. 0.45V is not linear. A large jump of the current density value appears from strain of -0.04% to -0.08%. To confirm the depletion approximation, the surface potential range should be between 0 and $E_g/2q$-ϕ_p. Figure 2b shows the variation of the surface potential versus the applied voltage under different strains from -0.08% to 0.08%. The surface potential increases as the strain changes from tensile strain to compressive strain. This is exactly in consistent with the results shown in Figure 2a. It should be emphasized that the current sensitivity upon applied strains is much larger

than the voltage sensitivity, particularly when the voltage value is above 0.4 V.

4. Numerical simulation

The current is continuous throughout the metal-insulator-semiconductor. Tunneling current can be described from metal to semiconductor, and drift-diffusion current is inside the semiconductor. The model can be solved numerically. Here we use a multi-physical software COMSOL to conduct the numerical calculations, which is a widely employed software allowing both equation-based customized numerical analysis and finite element modelling. Thus, the DC characteristics of the structure are obtained. According to the previous fundamental theoretical framework of piezotronics, the Gaussian profile is adopted to describe the dopant concentration function N as

$$N = -N_{Ap} - N_{Apmax} e^{-(\frac{z-l}{ch})^2} \quad (12)$$

where N_{Ap} is the p-type background doping concentration, N_{Apmax} is the maximum acceptor concentration, l is the length of semiconductor and ch is the doping fall-off constant.

The Shockley-Read-Hall recombination is taken as an example of carrier recombination mechanisms. The electrical contact of the electrodes with the semiconductor is supposed to be Ohmic contact, which means the carrier concentrations and electrical potential will have Dirichlet boundary conditions at the boundary with thermal equilibrium values same as in previous works.

In the simulation, it is assumed that the piezoelectric charges have a uniform distribution W_{piezo} at piezoelectric semiconductor, as shown in Figure 3a. In our simulation, the parameters are set as follows: The length of the semiconductor and insulator are 100 nm and 2.4 nm, respectively. The radius of the device is 10 nm. The piezoelectric material is wurtzite structure GaN with p-type background doping concentration N_{Ap} of 1×10^{15} cm^{-3}. The maximum acceptor doping concentration is 1×10^{17} cm^{-3}. The doping fall-off constant ch is 4.66 nm. The temperature is set to be 300 K. The relative dielectric constant of GaN is 8.9. The carrier lifetimes are $\tau_p = 0.01\mu s$ and $\tau_n = 0.01\mu s$. The electron and hole mobilities are $\mu_p = 350 cm^2V^{-1}s^{-1}$ and $\mu_n = 900 cm^2V^{-1}s^{-1}$.

Taking the above practical parameters of the MIS junction into the numerical model, the effect of piezoelectric charges on the I-V characteristic is shown in Figure 3b. Under compressive strains, the negative piezoelectric charges are created at the insulator-semiconductor interface,

which attract holes and repel electrons. While under tensile strains, the positive piezoelectric charges are created at the insulator-semiconductor interface which attract electrons to accumulate at the interface and repel holes along the semiconductor.

The distribution of electrons and holes across the semiconductor are illustrated in Figures 3c and 3d at different strains ranging from -0.08% to 0.08% under a fixed applied voltage of 2.2 V. Figure 3c shows the tendency of holes diffusing into the interior as the strains changes from +0.08% to -0.08%. When a tensile strain is applied, the electrons are attracted by positive piezoelectric charges to accumulate at the interface. As a compressive strain is applied, the created negative piezoelectric charges push the electrons away.

Moreover, we have looked into the I-V characteristics of the MIS structure under various background doping conditions and maximal doping conditions as Figure 4 shows. The strain was fixed at +0.08% and the default doping conditions are $N_{Ap\max} = 1\times10^{17}cm^{-3}$ and $N_{Ap} = 1\times10^{15}cm^{-3}$. Figure 4(a) depicts the current density-voltage curves as the maximal doping concentration changes from $1\times10^{16}cm^{-3}$ to $9\times10^{16}cm^{-3}$, very little change has been demonstrated. However when the background doping condition varies, the surface potential can be affected through the carrier concentration at the fixed voltage, which effectively tunes the I-V characteristics. Figure 4b shows the I-V characteristics of the MIS structure at various background doping concentrations. It is clearly observed from the numerical model that the background doping makes bigger impact on the I-V performance than the maximal doping concentration. Because piezo-charges induce energy band change, the DC characteristics are tuned by the piezo-charges. In our numerical model, not only the energy band change is considered, the carrier redistribution effect is also included.

For further investigation, the hole and electron distribution for different maximal doping conditions and background doping conditions are portrayed in Figures 5a-5d. It is seen from the results that the background doping plays more critical roles than the maximal doping conditions for both the electrons and holes distributions. The numerical analysis with practical parameters has revealed several key design specifications for the piezotronically tunable MIS devices, such as the strain condition and the background doping, which pave the way to real implementation of the structures in electronic systems. This work has filled in the gap of piezotronic effect used in semiconductor structures, as the MIS is equally important along with p-n junctions, metal-semiconductor contacts, and heterojunctions.

5. Conclusion

We have analyzed a one-dimensional simplified model of metal-insulator-semiconductor tunnel diode considering the piezotronic effect. The analytical solutions unveiled that the piezoelectric modulation can be realized through changing the band bending, which affects the carrier distribution in the semiconductor. The numerical simulation with designated geometrical and physical parameters of the proposed device was also conducted to support the analysis. The simulation results show that the piezotronic effect can be potentially introduced into the MIS tunnel diode to tune the performance and sensibility in the prospective devices. Furthermore, the analysis here provides a theoretical guide to the practical design of piezotronic MIS devices.

Acknowledgements

The authors are thankful for the support from Swansea University, and University of Electronic Science and Technology of China.

Figure captions:

Figure 1. Ideal metal-insulator-piezoelectric semiconductor contact with the presence of piezoelectric charges when applying positive voltage to metal. (a) charge distribution (b) electric field (c) potential distribution (d) band diagram of the structure.

Figure 2. (a) Current-voltage characteristics of ideal metal-insulator-piezoelectric semiconductor contact at strains ranging from -0.08% to +0.08%; (b) Variation of the surface potential versus the applied voltage V under different strains.

Figure 3. (a) Sketch of a metal-insulator-piezoelectric semiconductor contact; (b) Calculated current density curves voltage for different applied strains. Concentration distribution of holes (c) and electrons (d) at fixed voltage of 2.2V for various strains.

Figure 4. I-V characteristic of metal-insulator-piezoelectric semiconductor for different background doping density (a) and different maximum doping concentration (b).

Figure 5. Concentration distribution of holes (a) and electrons (b) at fixed voltage of 2.2V for various background doping conditions. Concentration distribution of holes (c) and electrons (d) at fixed voltage of 2.2V for different maximum doping conditions

Reference:

1. Wang, Z.L. and J.H. Song, *Piezoelectric nanogenerators based on zinc oxide nanowire arrays.* Science, 2006. **312**(5771): p. 242-246.
2. He, J.H., et al., *Piezoelectric gated diode of a single ZnO nanowire.* Advanced Materials, 2007. **19**(6): p. 781-+.
3. Zhou, J., et al., *Piezoelectric-Potential-Control led Polarity-Reversible Schottky Diodes and Switches of ZnO Wires.* Nano Letters, 2008. **8**(11): p. 3973-3977.
4. Wang, Z.L., *The new field of nanopiezotronics.* Materials Today, 2007. **10**(5): p. 20-28.
5. Wang, Z.L., *Nanopiezotronics.* Advanced Materials, 2007. **19**(6): p. 889-892.
6. Wang, Z.L., *Nanogenerators and nanopiezotronics.* 2007 Ieee International Electron Devices Meeting, Vols 1 and 2, 2007: p. 371-374.
7. Zhou, Y.S., et al., *Nano-Newton Transverse Force Sensor Using a Vertical GaN Nanowire based on the Piezotronic Effect.* Advanced Materials, 2013. **25**(6): p. 883-888.
8. Pan, C.F., et al., *Piezotronic Effect on the Sensitivity and Signal Level of Schottky Contacted Proactive Micro/Nanowire Nanosensors.* Acs Nano, 2013. **7**(2): p. 1803-1810.
9. Zhang, Z., et al., *Functional nanogenerators as vibration sensors enhanced by piezotronic effects.* Nano Research, 2014. **7**(2): p. 190-198.
10. Lee, M., et al., *A Hybrid Piezoelectric Structure for Wearable Nanogenerators.* Advanced Materials, 2012. **24**(13): p. 1759-1764.
11. Wu, W.Z., X.N. Wen, and Z.L. Wang, *Taxel-Addressable Matrix of Vertical-Nanowire Piezotronic Transistors for Active and Adaptive Tactile Imaging.* Science, 2013. **340**(6135): p. 952-957.
12. Yu, R.M., et al., *GaN Nanobelt-Based Strain-Gated Piezotronic Logic Devices and Computation.* Acs Nano, 2013. **7**(7): p. 6403-6409.
13. Pan, C.F., et al., *High-resolution electroluminescent imaging of pressure distribution using a piezoelectric nanowire LED array.* Nature Photonics, 2013. **7**(9): p. 752-758.
14. Wu, W.Z., et al., *Piezoelectricity of single-atomic-layer MoS2 for energy conversion and piezotronics.* Nature, 2014. **514**(7523): p. 470-+.
15. Zhang, B.C., et al., *Large-scale assembly of highly sensitive Si-based flexible strain sensors for human motion monitoring.* Nanoscale, 2016. **8**(4): p. 2123-8.
16. Cao, J., Q. Wang, and H. Dai, *Electromechanical properties of metallic, quasimetallic, and semiconducting carbon nanotubes under stretching.* Phys Rev Lett, 2003. **90**(15): p. 157601.
17. Shewchun, J., R. Singh, and M.A. Green, *Theory of Metal-Insulator-Semiconductor Solar-Cells.* Journal of Applied Physics, 1977. **48**(2): p. 765-770.
18. Pulfrey, D.L., *Mis Solar-Cells - Review.* Ieee Transactions on Electron Devices, 1978. **25**(11): p. 1308-1317.
19. Bayindir, M., et al., *Metal-insulator-semiconductor optoelectronic fibres.* Nature, 2004. **431**(7010): p. 826-829.
20. Lin, C.H. and C.W. Liu, *Metal-Insulator-Semiconductor Photodetectors.* Sensors, 2010. **10**(10): p. 8797-8826.
21. Strittmatter, R.P., et al., *Piezoelectrically enhanced capacitive strain sensors using GaN metal-insulator-semiconductor diodes.* Journal of Applied Physics, 2003. **94**(9): p. 5958-5963.
22. Ross, E.C. and J.T. Wallmark, *Theory of Switching Behavior of Mis Memory Transistors.* Rca Review, 1969. **30**(2): p. 366-&.

23. Singh, B., et al., *Electrical characteristics of metal-insulator-semiconductor diodes and transistors with space charge electret insulators: Towards nonvolatile organic memories.* Ieee Transactions on Dielectrics and Electrical Insulation, 2006. **13**(5): p. 1082-1086.
24. Fonash, S.J., *Outline and Comparison of Possible Effects Present in a Metal-Thin-Film-Insulator-Semiconductor Solar-Cell.* Journal of Applied Physics, 1976. **47**(8): p. 3597-3602.
25. Fonash, S.J., *Role of Interfacial Layer in Metal-Semiconductor Solar Cells.* Journal of Applied Physics, 1975. **46**(3): p. 1286-1289.
26. Zhang, Y., Y. Liu, and Z.L. Wang, *Fundamental Theory of Piezotronics.* Advanced Materials, 2011. **23**(27): p. 3004-3013.
27. Crowell, C.R. and S.M. Sze, *Current transport in metal-semiconductor barriers.* Solid-State Electronics, 1966. **9**: p. 1035-1048.
28. Sze, S.M., *Physics of semiconductor devices*, ed. 2nd. 1981, New York: Wiley.
29. Schottky, W., *Halbleitertheorie der Sperrschicht.* Naturwissenschaften, 1938. **26**(52): p. 843-843.
30. Bethe, H.A., *Theory of the Boundary Layer of Crystal Rectifiers.* MIT Radiation Lab. Report, 1942. **43**: p. 12.
31. Ikeda, T., *Fundamentals of Piezoelectricity*. 1996, Oxford, UK: Oxford University Press.
32. Freeman, L.B. and W.E. Dahlke, *Theory of Tunneling into Interface States.* Solid-State Electronics, 1970. **13**(11): p. 1483-&.
33. Card, H.C. and Rhoderic.Eh, *Studies of Tunnel Mos Diodes .1. Interface Effects in Silicon Schottky Diodes.* Journal of Physics D-Applied Physics, 1971. **4**(10): p. 1589-&.
34. Card, H.C. and Rhoderic.Eh, *Studies of Tunnel Mos Diodes .2. Thermal Equilibrium Considerations.* Journal of Physics D-Applied Physics, 1971. **4**(10): p. 1602-&.
35. Chattopadhyay, P. and A.N. Daw, *On the Current Transport Mechanism in a Metal-Insulator Semiconductor (Mis) Diode.* Solid-State Electronics, 1986. **29**(5): p. 555-560.
36. Ng, K.K. and H.C. Card, *A Comparison of Majority-Carrier and Minority-Carrier Silicon Mis Solar-Cells.* Ieee Transactions on Electron Devices, 1980. **27**(4): p. 716-724.
37. Tarr, N.G., D.L. Pulfrey, and D.S. Camporese, *An Analytic Model for the Mis Tunnel Junction.* Ieee Transactions on Electron Devices, 1983. **30**(12): p. 1760-1770.
38. Chu, K.M. and D.L. Pulfrey, *An Improved Analytic Model for the Metal Insulator-Semiconductor Tunnel Junction.* Ieee Transactions on Electron Devices, 1988. **35**(10): p. 1656-1663.
39. Doghish, M.Y. and F.D. Ho, *A Comprehensive Analytical Model for Metal-Insulator-Semiconductor (Mis) Devices - a Solar-Cell Application.* Ieee Transactions on Electron Devices, 1993. **40**(8): p. 1446-1454.
40. Doghish, M.Y. and F.D. Ho, *A Comprehensive Analytical Model for Metal-Insulator Semiconductor (Mis) Devices.* Ieee Transactions on Electron Devices, 1992. **39**(12): p. 2771-2780.
41. Lopezvillanueva, J.A., et al., *A Model for the Quantized Accumulation Layer in Metal-Insulator-Semiconductor Structures.* Solid-State Electronics, 1995. **38**(1): p. 203-210.
42. Vexler, M.I., et al., *A general simulation procedure for the electrical characteristics of metal-insulator-semiconductor tunnel structures.* Semiconductors, 2013. **47**(5): p. 686-694.
43. Harrison, W.A., *Tunneling from an Independent-Particle Point of View.* Physical Review, 1961.

123(1): p. 85-&.

44. Gray, P.V., *Tunneling from Metal to Semiconductors.* Physical Review, 1965. **140**(1A): p. A179-&.

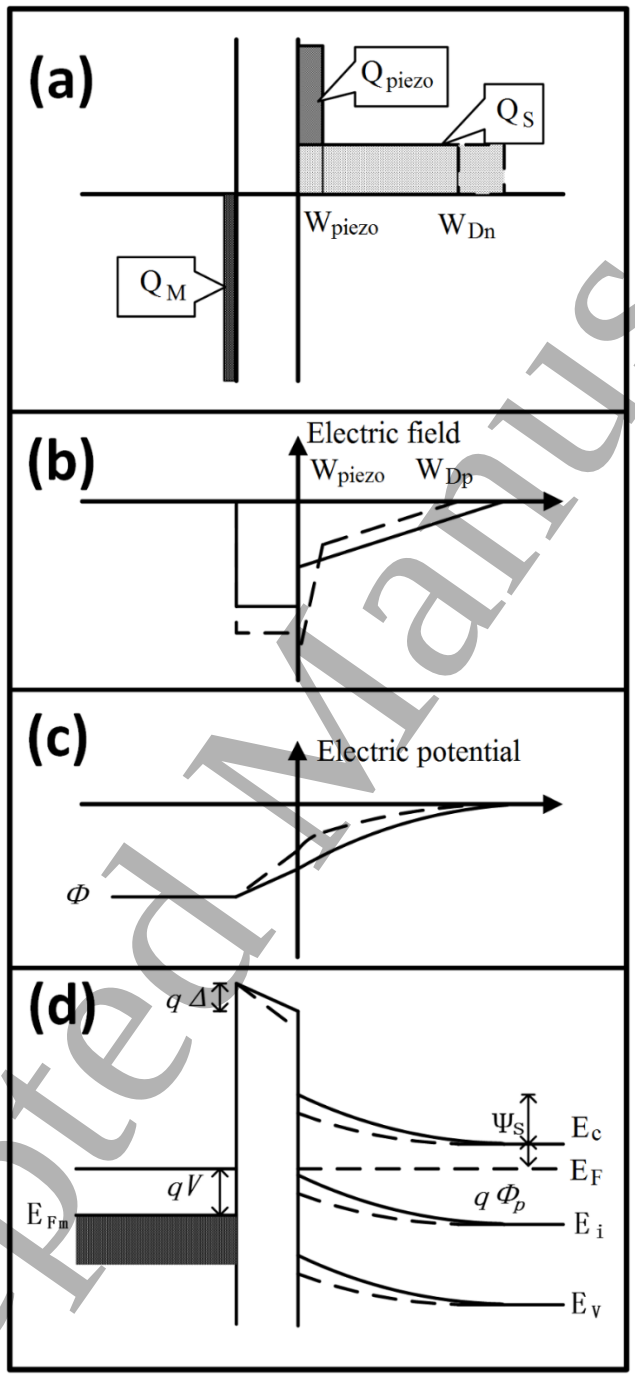

Fig. 1

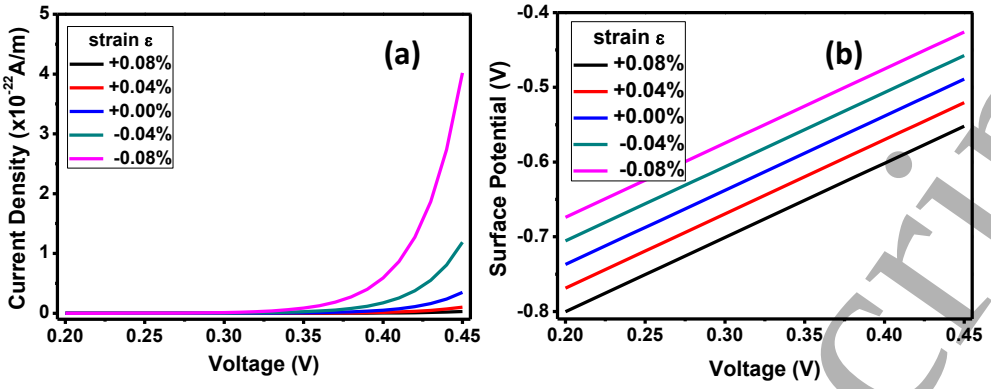

Fig.2

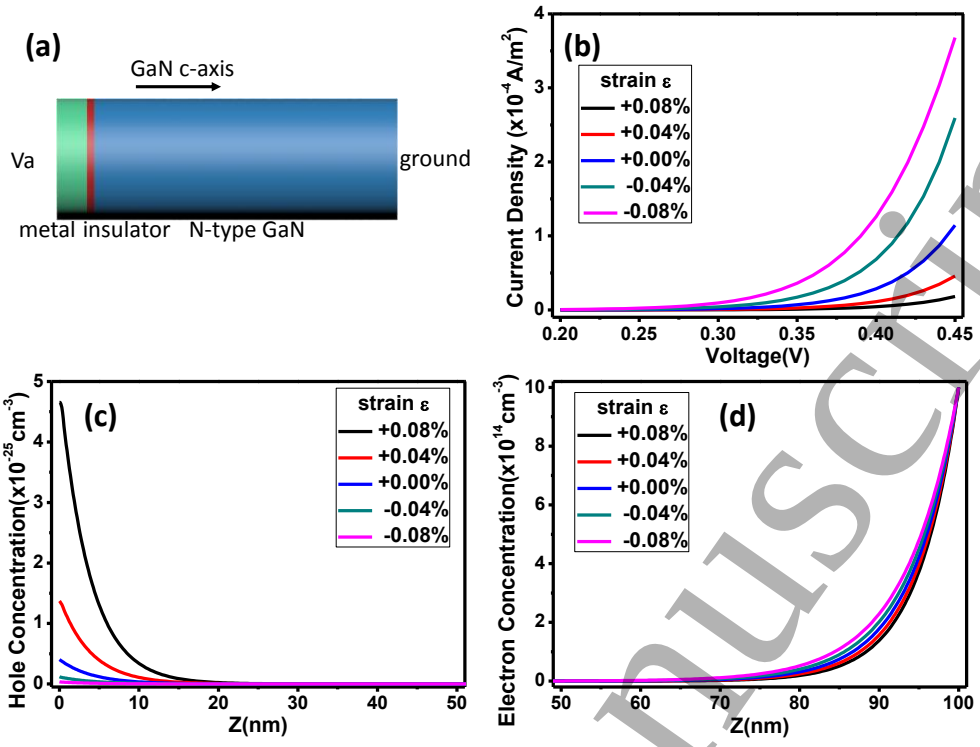

Fig.3

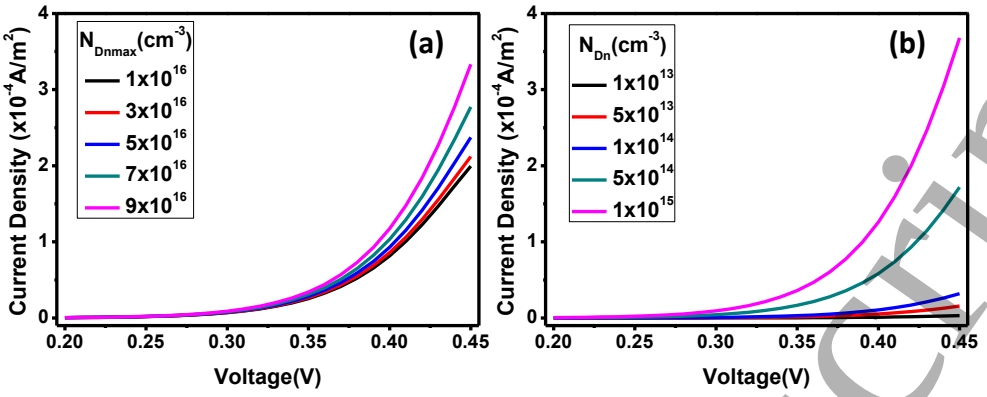

Fig.4

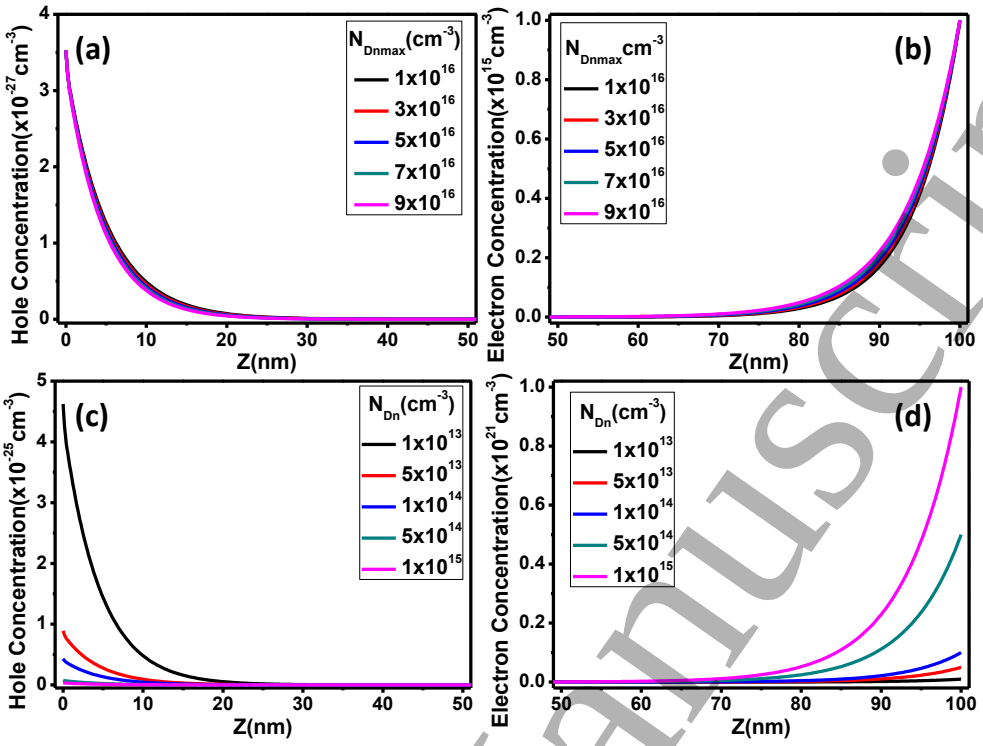

Fig.5